Forward-backward correlations in nucleus-nucleus collisions: Baseline contributions from geometrical fluctuations

V. P. Konchakovski,[1,2] M. Hauer,[1] G Torrieri,[3] M. I. Gorenstein,[2,4] and E. L. Bratkovskaya[4]
[1]*Helmholtz Research School, University of Frankfurt, Frankfurt, Germany*
[2]*Bogolyubov Institute for Theoretical Physics, Kiev, Ukraine*
[3]*Institut für Theoretische Physik, Goethe Universität, Frankfurt am Main, Germany*
[4]*Frankfurt Institute for Advanced Studies, Frankfurt, Germany*
(Received 20 December 2008; published 31 March 2009)

We discuss the effects of initial collision geometry and centrality bin definition on correlation and fluctuation observables in nucleus-nucleus collisions. We focus on the forward-backward correlation coefficient recently measured by the STAR Collaboration in Au + Au collisions at RHIC. Our study is carried out within two models: the Glauber Monte Carlo code with a "toy" wounded-nucleon model and the hadron-string dynamics (HSD) transport approach. We show that strong correlations can arise from averaging over events in one centrality bin. We, furthermore, argue that a study of the dependence of correlations on the centrality bin definition as well as the bin size may distinguish between these trivial correlations and correlations arising from new physics.

DOI: 10.1103/PhysRevC.79.034910 PACS number(s): 24.10.Lx, 24.60.Ky, 25.75.−q

I. INTRODUCTION

Correlations of particles between different regions of rapidity have for a long time been considered to be a signature of new physics. A shortening in the correlation length in rapidity has been thought to signal a transition to a quark-gluon plasma [1,2]. Conversely, the appearance of long-range correlations has been associated with the onset of the percolation limit, also linked to the QCD phase transition [3,4]. Recently, the correlations across a large distance in rapidity have also been suggested to arise from a color glass condensate [5–7]. The observation of such correlations in Au + Au collisions at RHIC energies by the STAR Collaboration [8,9] has therefore elicited a lot of theoretical interest.

The purpose of this work is to identify some *baseline* contributions to the experimentally observed correlations, contributions that do not depend on new physics. We will use models that incorporate event-by-event fluctuations in initial conditions to illustrate the effect of these contributions: a "toy" wounded-nucleon model and the hadron-string dynamics (HSD) transport model. We then argue that a study of the dependence of correlations on the centrality bin definition as well as the bin size may distinguish between these trivial correlations and correlations arising from new physics.

The paper is organized as follows. In Sec. II the main observables are introduced. In Secs. III and IV we study system size fluctuations and the resulting centrality dependence of correlations of two disconnected regions in momentum space within two different models: the Glauber Monte Carlo model (with no hadronic reinteractions or initial state dynamics) and the HSD transport model. Section V summarizes our study.

II. DEFINITION OF OBSERVABLES

The statistical properties of a particular sample of events can be characterized by a set of moments or cumulants of some observable. These properties depend upon a set of criteria that are used to select this sample. When applied to the context of heavy-ion collisions this translates to the construction of centrality bins of collision events from minimum-bias data. We will discuss the charged hadron multiplicities N_A and N_B in two symmetric intervals $\Delta\eta$ of pseudo-rapidity. After construction of the centrality bins, one can calculate the moments of a resulting distribution $P_c^{\eta_{\rm gap}}(N_A, N_B; \Delta\eta)$:

$$\left\langle N_A^k \cdot N_B^l \right\rangle_c^{\eta_{\rm gap}} \equiv \sum_{N_A, N_B} N_A^k N_B^l P_c^{\eta_{\rm gap}}(N_A, N_B; \Delta\eta). \qquad (1)$$

In Eq. (1) the subscript c denotes a particular centrality bin and the superscript $\eta_{\rm gap}$ denotes the separation of two symmetric intervals $\Delta\eta$ in pseudo-rapidity space where particle multiplicities N_A and N_B are measured. The correlation coefficient[1] is defined by

$$\rho \equiv \frac{\langle \Delta N_A \cdot \Delta N_B \rangle_c^{\eta_{\rm gap}}}{\sqrt{\langle (\Delta N_A)^2 \rangle_c^{\eta_{\rm gap}} \langle (\Delta N_B)^2 \rangle_c^{\eta_{\rm gap}}}} \qquad (2)$$

and measures how strongly multiplicities N_A and N_B—in a given centrality bin c for pseudo-rapidity separation $\eta_{\rm gap}$—are correlated. In Eq. (2), $\Delta N \equiv N - \langle N \rangle_c^{\eta_{\rm gap}}$ and $\langle (\Delta N_A)^2 \rangle_c^{\eta_{\rm gap}} = \langle (\Delta N_B)^2 \rangle_c^{\eta_{\rm gap}}$ for symmetric intervals.

The recent preliminary data on the forward-backward correlation coefficient (2) of charged particles by the STAR Collaboration [8,9] exhibit two striking features: 1. an approximate independence on the width of the pseudo-rapidity gap $\eta_{\rm gap}$ and 2. a strong increase of ρ with centrality.

III. GLAUBER MONTE CARLO MODEL

We use the PHOBOS Glauber Monte Carlo code [10] coupled to a "toy" wounded-nucleon model, referred to as GMC. The aim of this model is to emphasize two crucial aspects: (1) An

[1]We use a different notation from Refs. [8,9], denoting the correlation coefficient as ρ and reserving the letter b for the impact parameter.

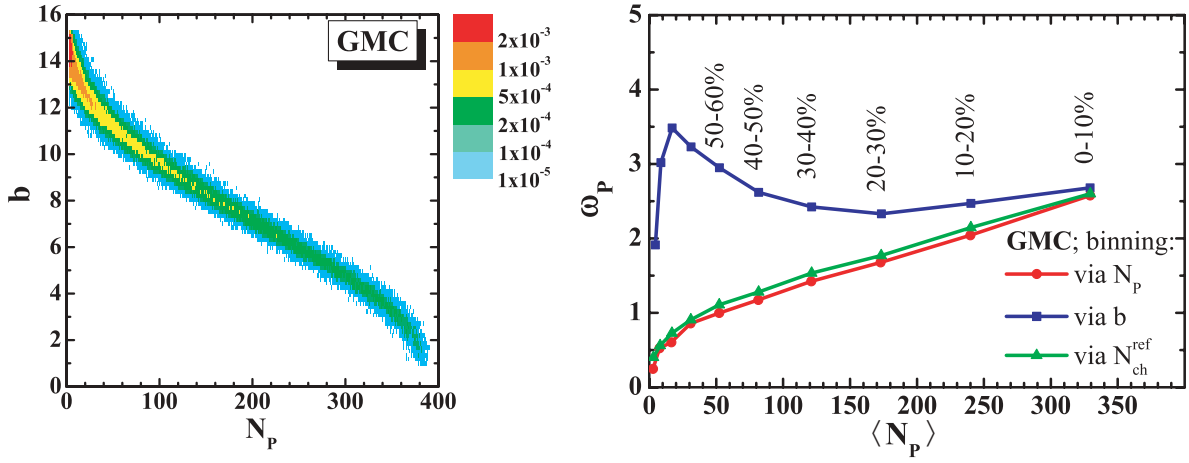

FIG. 1. (Color online) (Left) Histogram shows the distribution of events with fixed number of participating nucleons, N_P, and fixed impact parameter b in Au + Au collisions at $\sqrt{s} = 200$ GeV. (Right) The scaled variance ω_P of the distribution of participating nucleons in 10% bins as defined via b, N_P, and $N_{\rm ch}^{\rm ref}$.

averaging over different system sizes within one centrality bin introduces correlations and (2) the strength of these correlations depends on the criteria used for the centrality definition and on the size of the centrality bins.

Employing the Glauber code we model the distribution of the number of participating nucleons, N_P, in each nucleus-nucleus collision for given impact parameter b (cf. Fig. 1, left). This is done for Au + Au collisions with the standard Wood-Saxon profile and the nucleon-nucleon cross section of $\sigma_{NN} = 42$ mb. The "event" construction proceeds then in a two-step process. First, we randomly generate the total number of charged particles:

$$N_{\rm ch} = \sum_{i=1}^{N_P} n_{\rm ch}^i, \tag{3}$$

where the numbers of charged particles, $n_{\rm ch}^i$, per participating nucleon are generated by independently sampling a Poisson distribution with given mean value $\overline{n}_{\rm ch} = 10$. Second, these charged particles are randomly distributed according to a Gaussian in pseudo-rapidity space:

$$\frac{dN_{\rm ch}}{d\eta} \propto \exp\left(-\frac{\eta^2}{2\sigma_\eta}\right), \tag{4}$$

where $\sigma_\eta = 3$ defines the width of the pseudo-rapidity distribution. Hence, in each single event there are no correlations between the momenta of any two particles. Note that numerical values of $\overline{n}_{\rm ch}$ and σ_η are fixed in a way to have a rough correspondence with the data on charged particle production at $\sqrt{s} = 200$ GeV.

In Fig. 1 (left) we show the GMC event distribution in the (b, N_P)-plane. For each of these events we randomly generate the number of charge particles, $N_{\rm ch}$, and their η distribution according to Eqs. (3) and (4), respectively. The construction of centrality classes can now be done in several ways. Here we focus on the following criteria: via impact parameter b, via the number of participating (wounded) nucleons, N_P, and via the charged particle multiplicity $N_{\rm ch}^{\rm ref}$ in the midrapidity window $|\eta| < 1$.

In the case where one chooses the number of participating nucleons, N_P, for the centrality definition, one takes vertical cuts in Fig. 1 (left); when choosing the impact parameter b, one takes horizontal cuts. Hence, depending on the centrality definition, one may assign a particular event (characterized by N_P and b) to two different centrality bins.

In Fig. 1 (right) we show the resulting scaled variance,

$$\omega_P \equiv \frac{\langle (\Delta N_P)^2 \rangle_c}{\langle N_P \rangle_c}, \tag{5}$$

of the underlying distribution of the number of participating nucleons, N_P, in each centrality bin. Using the centrality selection via impact parameter b, which is a only theoretically available trigger, one generally obtains a rather wide distribution of participating nucleons in each bin. The lines for centrality selections via $N_{\rm ch}^{\rm ref}$ and via N_P are similar owing to the event construction with Eqs. (3) and (4). An interesting feature of the GMC model is that ω_P increases with centrality for the selection via N_P. This result of the GMC model seems to have a rather general origin.

We now investigate the sensitivity of the forward-backward correlation signal as a function of the separation $\eta_{\rm gap}$ of two narrow intervals ($\Delta\eta = 0.2$) on the centrality definition. This is done for the 10% centrality defined via N_P, via b, and via $N_{\rm ch}^{\rm ref}$. The results are shown in Fig. 2.

In the GMC we can identify the number of participating nucleons, N_P, with the system size, and ω_P as the measure for system size fluctuations. Having a large system as measured by N_P implies a large number of charged particles, $N_{\rm ch}$. In GMC they are distributed independently in pseudo-rapidity space. Conversely, an event with small N_P contains only few charged particles. By grouping the collision events into 10% centrality bins one finds rather large N_P fluctuations in one specific bin. The averaging over different states in the centrality bin introduces correlations between any two regions of pseudo-rapidity. Small systems will have few particles on the left and few particles on the right with respect to midrapidity. Large systems will have many particles on the left and many particles

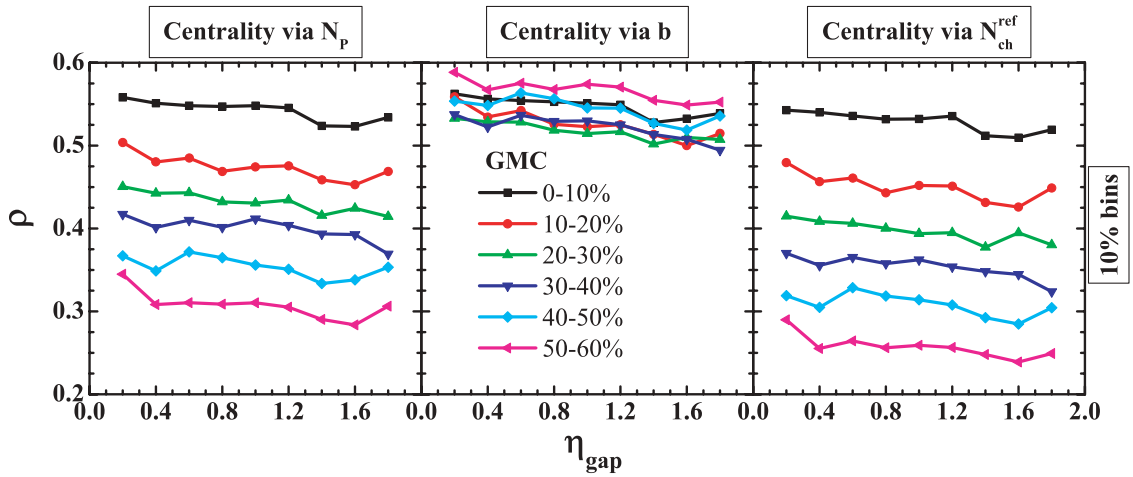

FIG. 2. (Color online) The forward-backward correlation coefficient ρ for 10% centrality classes defined via N_P (left), via the impact parameter b (middle), and via the multiplicity in the central rapidity region $N_{\rm ch}^{\rm ref}$ (right).

on the right. But this just means a nonzero forward-backward correlations. From the definition [Eq. (2)] one finds a positive correlation coefficient ρ owing to averaging over system sizes.

Note that centrality selections via N_P and via $N_{\rm ch}$ give essentially the same results for ρ in the GMC (cf. left and right panels of Fig. 2). Using the impact parameter b for the centrality definition generates centrality bins with almost constant ρ, as seen in Fig. 2 (middle). This is due to a rather flat dependence of ω_P on the centrality defined via b, as shown in Fig. 1 (right). In the GMC model the apparent ordering of ρ values with respect to centrality bins originates from the width of the underlying distribution in the number of wounded nucleons in each bin (i.e., from the values of ω_P).

The measured and apparently strong forward-backward correlations can be accounted for by a "toy" model such as the GMC, provided it produces particles over the whole rapidity range and includes strong enough event-by-event fluctuations of N_P. The next section will show that an introduction of dynamics and hadron reinteractions within the HSD does not alter these conclusions significantly.

IV. HSD TRANSPORT MODEL SIMULATIONS

A physically more reasonable scenario, which however also does not include any new physics (such as color glass condensate or quark-gluon plasma), can be obtained in the HSD transport approach [11–13]. The HSD approach has been used for the description of pA, πA, and AA collisions from SIS to RHIC energies [14,15]. In this model, N, Δ, $N^*(1440)$, $N^*(1535)$, and Λ, Σ, Σ^*, Ξ, Ξ^*, and Ω hyperons as well as their antiparticles are included on the baryonic side, whereas the 0^- and 1^- octet states are incorporated in the mesonic sector. Inelastic baryon-baryon (and meson-baryon) collisions with energies above $\sqrt{s}_{\rm th} \simeq 2.6$ GeV (and $\sqrt{s}_{\rm th} \simeq 2.3$ GeV) are described by the FRITIOF string model [16] whereas low-energy hadron-hadron collisions are modeled in line with experimental cross sections. As pre-hadronic degrees of freedom the HSD includes "effective" quarks (antiquarks) and diquarks (antidiquarks) that interact with cross sections in accordance with the constituent quark model.

As before within GMC, the HSD events are generated according to a uniform distribution, $N_{\rm ev}(b) \sim b$. The resulting distribution of events in the (N_P, b)-plane is similar to the GMC result depicted in Fig. 1 (left).

In Fig. 3 we show the distribution of events with fixed N_P for both models. The vertical lines indicate 10% centrality bins as defined by the N_P distribution. Note that the peripheral part of the distribution also determines the centrality binning and the real bin widths. This is crucial for most central collisions where the number of events is small. Slight uncertainties in the peripheral "tail" of the distribution lead to large errors in the sizes of most central bins and hence to large changes in results for fluctuations and correlations.

In contrast to the STAR data, we use in the HSD simulations the charged particle reference multiplicity $N_{\rm ch}^{\rm ref}$ in the same pseudo-rapidity range $|\eta| < 1$ for all values of $\eta_{\rm gap}$. This procedure introduces a systematic bias, since the pseudo-rapidity regions for the measured multiplicity in a small $\Delta\eta$ window (signal) and for the reference multiplicity partially overlap. This bias, however, is small and does not affect any of our conclusions.

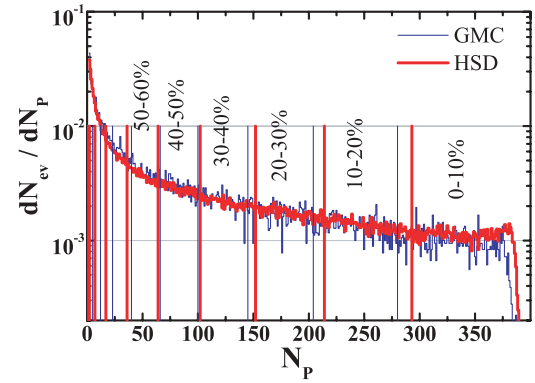

FIG. 3. (Color online) The HSD and GMC distributions of events over N_P. The vertical lines indicate 10% centrality bins.

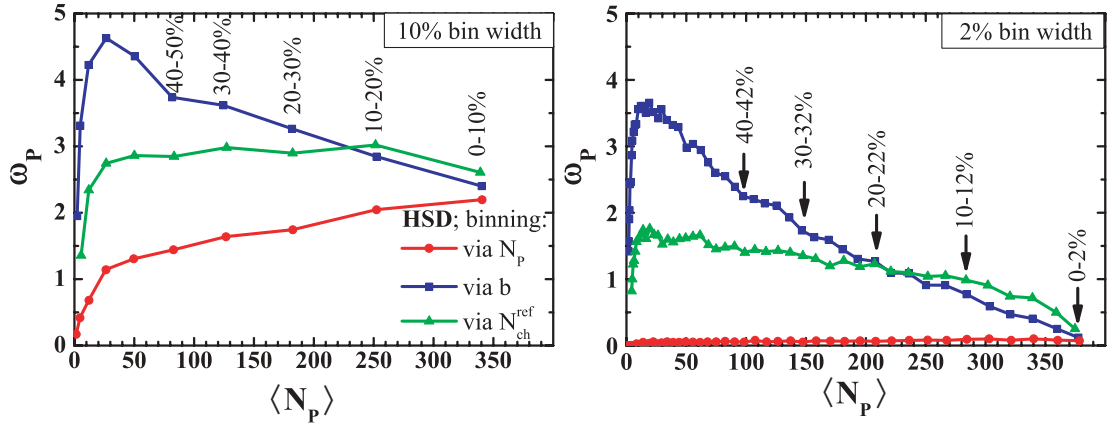

FIG. 4. (Color online) The HSD results for the fluctuations ω_P as a function of the mean value $\langle N_P \rangle$ of the participating nucleons within bins as defined via b, N_P, and $N_{\rm ch}^{\rm ref}$. The left panel corresponds to a 10% and the right to a 2% bin width.

In Fig. 4 we show the scaled variance of the underlying N_P distribution for 10% (left) and 2% (right) centrality bins defined via different centrality triggers within HSD. The results for 10% bins can be compared with the scaled variance ω_P in the GMC model in Fig. 1 (right). Fluctuations of the number of participants, as well as their average values, are similar in both HSD and GMC models when the centrality bins are defined via N_P. These quantities are completely defined by the N_P distribution, which is similar in both models (Fig. 3). Binning via the impact parameter b in HSD, as well as in GMC, gives decreasing fluctuations in the participant number with increasing collision centrality. The results for 10% bins defined via the reference multiplicity are rather different in the GMC and HSD models. In GMC the charged multiplicity distribution is implemented according to Eqs. (3) and (4). Hence, the results obtained by binning via the reference multiplicity follow the line obtained by binning via N_P. In contrast to the GMC, in the HSD simulations the average number of charged particles, $\overline{n}_{\rm ch}$, per participating nucleon is not a constant but increases with N_P. Additionally, the shape of the rapidity distribution is also different in different centrality bins. These two effects lead to different values of ω_P in the centrality bins defined via $N_{\rm ch}^{\rm ref}$ in the GMC and HSD models.

One comment is appropriate here. It was argued in Ref. [17] that any centrality selection in nucleus-nucleus collisions is equivalent to the geometrical one via impact parameter b. This result was obtained in Ref. [17] by neglecting the fluctuations at a given value of b. Thus, different centrality selection criteria give indeed the same *average* values of physical observables. However, they may lead to rather different fluctuations of these observables in the corresponding centrality bins (cf. equal values of $\langle N_P \rangle$ and different values of ω_P for different centrality selections presented in Fig. 4).

When considering smaller centrality bins (2% in Fig. 4, right) the fluctuations in the participant number become smaller and more strongly dependent on the definition of the binning.

Figure 5 summarizes the dependence of the forward-backward correlation coefficient ρ as a function of $\eta_{\rm gap}$ on the bin size and centrality definition within the HSD model. The dependence of ρ on $\eta_{\rm gap}$ is almost flat, reflecting a boost-invariant distribution of particles created by string breaking in the HSD. The right top panel of Fig. 5 demonstrates also a comparison of the HSD results with the STAR data [8,9]. One observes that the HSD results systematically exceed the STAR data. However, the main qualitative features of the STAR data—an approximate independence of the width of the pseudo-rapidity gap $\eta_{\rm gap}$ and a strong increase of ρ with centrality—are fully reproduced by the HSD simulations.

The correlation coefficient ρ largely follows the trend of the participant number fluctuations ω_P as a function of centrality. The actual results, however, strongly depend on the way of defining the centrality bins. For instance, choosing smaller centrality bins leads to weaker forward-backward correlations, a less pronounced centrality dependence, and a stronger dependence on the bin definition. The physical origin for this is demonstrated in Fig. 6. As the bin size becomes comparable to the width of the correlation band between N_P and $N_{\rm ch}^{\rm ref}$, the systematic deviations of different centrality selections become dominant: The same centrality bins defined by N_P and by $N_{\rm ch}^{\rm ref}$ contain different events and may give rather different values of forward-backward correlation coefficient ρ.

It should be underlined that these properties are specific to the *geometric* nature of the correlations analyzed here. If the observed fluctuations are of *dynamical* origin (for example, arising from the quantum fluctuations of coherent fields created in the first fm/c of the system's lifetime as in Refs. [5,6]), there are no evident reasons why they should strongly depend on centrality bin definitions and bin sizes. Thus, the experimental analysis for different bin sizes and centrality definitions—as performed here—may serve as a diagnostic tool for an origin of the observed correlations. A strong specific dependence of the correlations on bin size and centrality definition would signify their geometrical origin.

V. SUMMARY

In conclusion, we have presented a study of the system size event-by-event fluctuations causing the rapidity forward-backward correlations in relativistic heavy-ion collisions. Our analysis has been based on two independent models—a "toy"

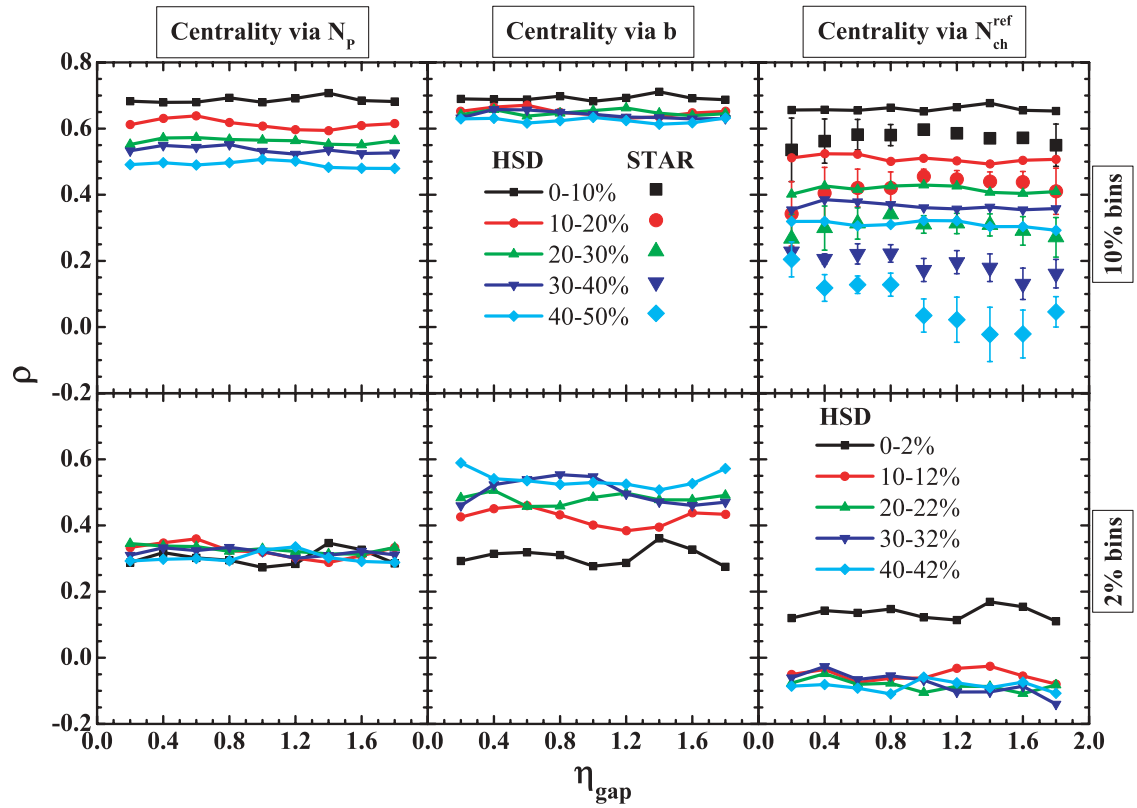

FIG. 5. (Color online) The HSD results for the forward-backward correlation coefficient ρ for 10% (top) and 2% (bottom) centrality classes defined via N_P (left), via impact parameter b (center), and via the reference multiplicity $N_{\rm ch}^{\rm ref}$ (right). The symbols in the top right panel present the STAR data in Au + Au collisions at $\sqrt{s} = 200$ GeV [8,9].

wounded-nucleon model realized as a Glauber Monte Carlo event generator and the microscopic HSD transport approach. We have shown that strong forward-backward correlations arise from an averaging over many different events that belong to one 10% centrality bin. In contrast to average multiplicities, the resulting fluctuations and correlations depend strongly on the specific centrality trigger. For example, the centrality selection via impact parameter b used in most theoretical calculations and via $N_{\rm ch}^{\rm ref}$ used experimentally lead to rather different values of ω_P and ρ and their dependence on centrality.

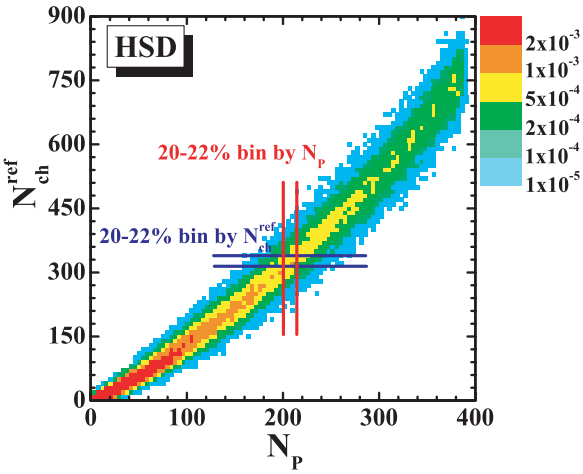

FIG. 6. (Color online) Histogram showing the distribution of HSD events with fixed number of participating nucleons, N_P, and fixed reference charge particle multiplicity $N_{\rm ch}^{\rm ref}$. The same centrality class (20%–22% as an example) defined in various ways contains different events.

In the HSD model the N_P distribution is similar to that in the GMC. It also includes the fluctuations in the number of strings and the fluctuations in the number of hadrons from individual string fragmentation. The HSD simulations reveal strong forward-backward correlations and reproduce the main qualitative features of the STAR data in Au + Au collisions at RHIC energies [5,6].

The forward-backward correlations can be studied experimentally for smaller size centrality bins defined by $N_{\rm ch}^{\rm ref}$. When the size of the bins decreases, the contribution of geometrical fluctuations discussed in our paper should lead to weaker forward-backward correlations and to a less pronounced centrality dependence.

Let us stress that the geometrical fluctuations discussed in our paper are in fact present in all dynamical models of nucleus-nucleus collisions. Thus, they should be carefully taken into account before any discussion of new physical effects. We hope that a future experimental analysis in the direction examined here will clarify whether the observed correlations by the STAR Collaboration at RHIC contain really additional contributions from new physics.

ACKNOWLEDGMENTS

The authors are grateful for useful discussions with W. Broniowski, M. Gaździcki, M. Mitrovski, T. Schuster, and P. Steinberg. G. T. acknowledges the LOEWE foundation, the 'HIC for FAIR' program, and the ITP and FIAS of Johann Wolfgang Goethe University for support. This work was in part supported by the Program of Fundamental Researches of the Department of Physics and Astronomy of NAS, Ukraine.

[1] A. Bialas and R. B. Peschanski, Nucl. Phys. **B273**, 703 (1986).
[2] S. Jeon, L. Shi, and M. Bleicher, Phys. Rev. C **73**, 014905 (2006).
[3] N. Armesto, M. A. Braun, E. G. Ferreiro, and C. Pajares, Phys. Rev. Lett. **77**, 3736 (1996).
[4] M. A. Braun and C. Pajares, Phys. Rev. Lett. **85**, 4864 (2000).
[5] N. Armesto, L. McLerran, and C. Pajares, Nucl. Phys. **A781**, 201 (2007).
[6] T. Lappi and L. McLerran, Nucl. Phys. **A772**, 200 (2006).
[7] A. Dumitru, Y. Nara, B. Schenke, and M. Strickland, Phys. Rev. C **78**, 024909 (2008).
[8] T. J. Tarnowsky (STAR Collaboration), PoS C **POD07**, 019 (2007).
[9] T. Tarnowsky, R. Scharenberg, and B. Srivastava, Int. J. Mod. Phys. E **16**, 1859 (2007).
[10] B. Alver, M. Baker, C. Loizides, and P. Steinberg, arXiv:0805.4411 [nucl-ex]. The PHOBOS Glauber Monte Carlo code is available at http://www.hepforge.org/downloads/tglaubermc.
[11] W. Ehehalt and W. Cassing, Nucl. Phys. **A602**, 449 (1996).
[12] E. L. Bratkovskaya and W. Cassing, Nucl. Phys. **A619**, 413 (1997).
[13] W. Cassing and E. L. Bratkovskaya, Phys. Rep. **308**, 65 (1999).
[14] W. Cassing, E. L. Bratkovskaya, and S. Juchem, Nucl. Phys. **A674**, 249 (2000).
[15] E. L. Bratkovskaya *et al.*, Phys. Rev. C **69**, 054907 (2004).
[16] B. Anderson, G. Gustafson, and H. Pi, Z. Phys. C **57**, 485 (1993).
[17] W. Broniowski and W. Florkowski, Phys. Rev. C **65**, 024905 (2002).